



Particle Image Velocimetry and Finite Volume Method Study of Bi-leaflet Artificial Heart Valve

H. Abu Bakar¹, A. Abas^{1†}, N. Hafizah Mokhtar¹, N. Razak² and M. Najib Bin Abdul
Hamid³

¹ School of Mechanical Engineering, Universiti Sains Malaysia, Engineering Campus, 14300 Nibong Tebal,
Penang, Malaysia

² School of Aerospace Engineering, Universiti Sains Malaysia, Engineering Campus, 14300 Nibong Tebal,
Penang, Malaysia

³ Mechanical Sect. Universiti Kuala Lumpur Malaysia Spanish Institute, Kulim Hi-Tech Park, 09000 Kulim, Kedah

[†]Corresponding Author Email: [aizatabas@usm.my](mailto: aizatabas@usm.my)

(Received January 21, 2018; accepted April 8, 2018)

ABSTRACT

The key feature of the bi-leaflet valve is the geometry of the two leaflets, which can be crucial in determining the flow field. In this paper, observations were made on the flow pattern of the blood through the use of bi-leaflet type mechanical prosthetic valve (MHV). Finite volume method (FVM) analysis was conducted using fluid-structure interaction (FSI) method that solved on a dynamic mesh. In terms of the validation, particle image velocimetry (PIV) was used to verify the findings obtained from FVM analysis. The results of velocity and vorticity were the main parameters to be compared. Based on the findings, the results computed for the leaflets motion and the flow field using FVM was found to be in agreement with PIV experimental data. The pressure obtained for the simulation is in the range of 10,666 – 16,000 Pa, which is an ideal and healthy blood pressure level of human. The vorticity was observed to be formed behind the valve with DVI value of 1.275 (simulation) and 1.457 (experiment), lower than the expected range for a normal DVI in mitral valve. The maximum shear stress achieved (22.5481 Pa) is in the range of platelets activation, which could lead to thrombus formation. The maximum Von Mises stress was found to be at the hinge region of the bi-leaflet valve. These results will serve as a basis for valve design to improve the hemodynamic properties of the heart valve.

Keywords: Mechanical heart valve; Particle image velocimetry; Fluid-structure interaction; Dynamic mesh.

NOMENCLATURE

Nomenclature should be in alphabetic order (A – Z) and Greek letters should follow after Latin letters in alphabetic order ($\alpha \beta \dots$)

| | | | |
|-------|----------------------------|----------------------|----------------------------------|
| DVI | Dopler Velocity Index | <i>Greek letters</i> | |
| g | gravity | α | diffusion parameter |
| h | height | γ | diffusion coefficient |
| n | power index | ρ | density |
| P | pressure | μ_{eff} | effective viscosity |
| Re | Reynold number (-) | μ_0 | viscosity at zero shear rate |
| S_p | surface area | μ_{inf} | viscosity at infinite shear rate |
| V_p | volume | $\bar{\tau}$ | shear stress |
| T | temperature | λ | Relaxation time |
| t | time | v_{inlet} | velocity inlet |
| u | mesh displacement velocity | | |

1. INTRODUCTION

Valvular heart disease is affecting more than 100 million people globally and in some severe cases can lead to significant morbidity and mortality rate (Dangas, Weitz, Giustino, Makkar, & Mehran,

2016). Del Gaudio, Gasbarroni, and Romano (2016), predicted a rise in these conditions because of the increase in degenerative pathologies and persistent burden of rheumatic fever. Prosthetic heart valve becomes one of the solution to treat the disease. According to Misawa (2015), around 5,452

mechanical valve replacements have been implanted to the patients suffering from valvular heart disease in the year 2011 alone. Mechanical heart valve (MHV) are made from material such as titanium and carbon (Harris, Croce, & Cao, 2015). The advantage of MHV is its outstanding durability, yet due to the hemodynamic characteristic of the blood, MHV could initiate damage to the blood components (Dangas *et al.*, 2016; Harris *et al.*, 2015). Consequently, this can lead to thrombosis formation. Thromboembolism is a major issue for patients with MHV replacement. To overcome it, the patients are required to undergo anticoagulant therapy for the rest of their life (Sato, Harasaki, Wika, Soloviev, & Lee, 2003). The downside of the therapy is it can induce hemorrhagic complication, that will result in problem such as major bleeding (Sato *et al.*, 2003). Therefore, the necessity to resolve thrombosis formation in MHV without the needs to go through such consistent therapy is highly desired.

Hedayat, Asgharzadeh, and Borazjani (2017), stated that thrombosis is initiated by platelet activation, which is dependent on the induced-shear stress and its exposure time. These factors, caused by the dynamic and complex flow of the blood, are the main culprit for the clinical complications that arise from the implantation of the MHV (Le & Sotiropoulos, 2013). To accurately study the flow behaviors, numerical approach through computational fluid dynamics (CFD) has become one of the preferred option by many researchers (Al-Atabi & Lim, 2013; Luraghi *et al.*, 2017). Fluid structure interactions (FSI) between the blood and valve are essential in producing a more precise simulation outcomes (Arefin, 2017). FSI has been implemented broadly in the hemodynamic studies and changes in physiological structures (Arefin, 2017). Its approach is complicated but capable to produce realistic results by coupling the interaction between the blood and tissue (Su *et al.*, 2014). Al-Atabi and Lim (2013), performed 2-D model simulation of blood flowing through the mitral valve using ANSYS FLUENT. They succeeded in visualizing the vortices formation that occur, which in the end, could lead to high shear stress. Luraghi *et al.* (2017), claimed that a number of computational studies on prosthetic heart valves simply considers the hydrostatic pressures acting on the structure domain. In their study, they compared the stress generated for both FSI and finite element (FE) simulations during maximum closing of the valve. The FSI model successfully predicted larger stress than pure FE model, proving that FE model was underestimated the stress value (Luraghi *et al.*, 2017). Hong and Kim (2011), used FSI method to investigate the effect of rotation angle of the MHV on the blood flow and leaflets' behavior. The flow recirculation regions obtained in different sinuses produced asymmetrical blood flow (Hong & Kim, 2011). Hence, this has shown the importance of FSI in the study involving both fluid and structure dynamics to avoid underestimation of the obtained results. Most of the studies conducted using numerical simulations did not include validation of the implement FSI codes which may lead to some

ambiguity on the computed results. Given the importance of having highly accurate computed data, the need for validation with experimental observation becomes a necessity. The use of experimental procedure such as Particle Image Velocimetry (PIV) is capable of providing such validation capability with numerical simulation given its state-of-the-art flow tracking capability as the flow progresses. This is very important in identifying the improvement required on the artificial heart implanted.

PIV technique is not an uncommon procedure especially in fluid dynamics study and in bioengineering study relating to blood flow. The technique has been developed since the early 1980's (Mokhtar, Abas, Teong, & Razak, 2016), and it is considered as a non-intrusive optical technique that is capable in providing measurements of the instantaneous velocity vector field in a plane located in the flow region of interest (Ducci, Pirisi, Tzamtzis, & Burriesci, 2016). The PIV setup is correlated with optical access of the designed in-vitro testing loops to exactly simulate the heart and vascular system (Kaminsky *et al.*, 2008). The complex condition such as unsteady periodically generated flow can be achieved through PIV by averaged phase locked or measurement with high temporal and spatial resolution (Kaminsky *et al.*, 2008). Ducci *et al.* (2016), did a 2-D PIV experiment to study the unphysiological flows that could contribute to thromboembolism. Del Gaudio *et al.* (2016), implemented the PIV method to evaluate the performance of biodegradable electro-spun heart valve prosthesis, which in the end, attained the correct functionality of the device. This is then supported by the formation of vortex structures at the end of the three cusps, observed in the PIV experiment. Bark *et al.* (2016), observed the flow fields generated by different textile fabrication techniques through time-resolved PIV technique. Mokhtar *et al.* (2016), performed the PIV experiment to analyze the effect of stent placement on the flow pattern, velocity, and pressure with hope to reduce the size of the aneurysm issue.

However, the FSI approach that is supported by validation of the experimental data in studying the effect of hemodynamic flow through MHV, especially for the case of mitral valve study is still limited in number. Nguyen *et al.* (2012) studied the intraventricular flow of the bi-leaflet MHV at the mitral position, and is only focused on simulation without experimental validation. Annerel, Claessens, Degroote, Segers, and Vierendeels (2014) did performed FSI simulation together with PIV experiment as a method of validation, but their study was focused on aortic position of the heart valve. Additionally, Su *et al.* (2014) focuses more on numerical simulation for both mitral and aortic valves using FSI method. No experimental validation on their behalf is done to compare the results obtained from their simulation. Therefore, the aim of the current paper is to combine the best features of FSI simulation and PIV experiment in providing comprehensive and reliable

hemodynamic flow of the blood through a bi-leaflet MHV at mitral position. This will serve as a basis for valve design in order to improve the hemodynamic of the heart valve.

2. FLUID STRUCTURE INTERACTION (FSI) SETUP

Fluid Structure Interaction (FSI) is a multi-physics coupling between the laws that describe the fluid dynamics and the structural mechanics. This condition is characterized by the interactions between deformable or moving structure and the surrounding or the internal fluid flow. In this study, two-way FSI is used, which is correlated with the mechanical model and the CFD model analysis results. Figure 1 exhibits the general overview of two-way FSI setup procedure.

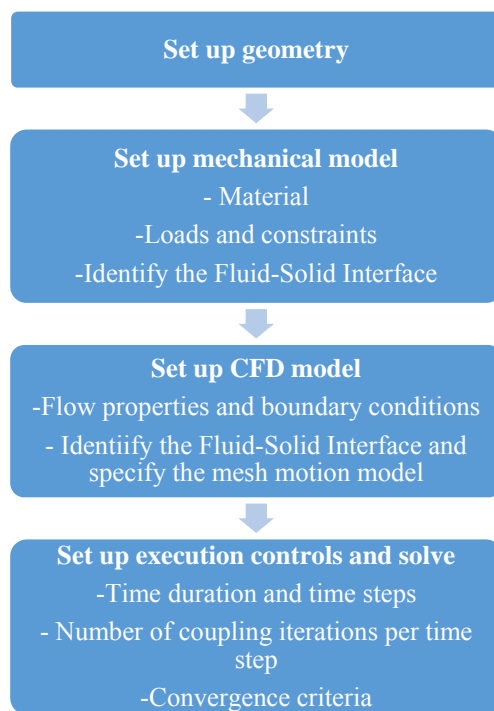


Fig. 1. General overview of two-ways FSI setup procedure

2.1 Governing Equations

Before commencing a CFD simulation, it is important to look at the governing equations underlying the physics taken place. The fundamental governing equations involved are the continuity equation and the Navier-Stokes equations.

Continuity equation

$$\frac{\partial \rho}{\partial t} + \nabla \cdot (\rho \mathbf{v}) = 0 \quad (1)$$

Since blood is considered as incompressible fluid, the continuity equation reduces to:

$$\nabla \cdot \mathbf{v} = 0 \quad (2)$$

Navier-Stokes equations

$$\rho \left(\frac{d\mathbf{v}}{dt} + \mathbf{v} \cdot \nabla \mathbf{v} \right) = -\nabla p + \mu \nabla^2 \mathbf{v} + \mathbf{f} \quad (3)$$

In Navier-Stokes equations, the viscosity coefficient, μ is not a constant. It is a function of shear rate. Blood will be less viscous as the shear rate increased. This phenomenon is known as shear thinning. Therefore, the Carreau model (Nguyen *et al.*, 2012) will be employed to simulate the blood viscosity. The mathematical formulation of Carreau model is:

$$\mu_{eff}(\dot{\gamma}) = \mu_{inf} + (\mu_0 - \mu_{inf}) (1 + (\lambda \dot{\gamma})^2)^{\frac{n-1}{2}} \quad (4)$$

Where:

μ_{eff} = effective viscosity

μ_0 = viscosity at zero shear rate (Pa·s)

μ_{inf} = viscosity at infinite shear rate (Pa·s)

λ = relaxation time (s)

n = power index

For the case of blood,

$\mu_0 = 0.056$ (kg/m·s)

$\mu_{inf} = 0.0035$ (kg/m·s)

$\lambda = 3.313$ (s)

$n = 0.3568$

Material coefficients

2.2 Boundary Conditions (BC)

The mammalian blood flow is pulsatile and cyclic in nature. Consequently, the velocity at the inlet is not set to be a constant, rather it is a time varying periodic profile. The pulsatile profile within each period is a combination of two phases which are systolic and diastolic phase. During the systolic phase, the velocity at the inlet varies in a sinusoidal pattern. The sine wave during the systolic phase has a peak velocity of 0.5 m/s and minimum velocity of 0.1 m/s. Assuming a rapid heartbeat rate of 120 beat per minute, the duration of each period is 0.5 s. The model for pulsatile blood flow was proposed by Sinnott, Cleary, and Prakash (2006). Figure 2 shows the inlet velocity profile in two periods.

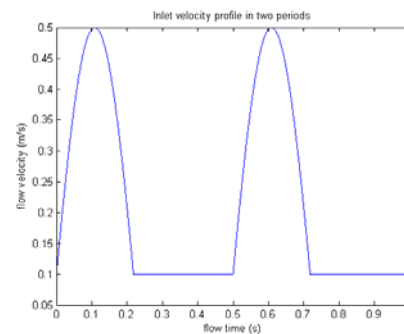


Fig. 2. Inlet velocity profile in two periods

To illustrate the profile clearly, a mathematical description is also given as follow:

$$v_{inlet}(t) = \begin{cases} 0.5 \sin[4\pi(t + 0.0160236)] & 0.5n < t \leq 0.5n + 0.218 \\ 0.1 & 0.5n + 0.218 < t \leq 0.5(n+1) \end{cases}$$

Where $n = 0, 1, 2, \dots$

Outlet BC

The systolic and diastolic pressure of a healthy human is around 120 mmHg and 80 mmHg respectively. Hence, the average pressure of the two phases (100 mmHg) will be used as the static gauge pressure at the outlet.

Wall BC

The easiest BC to determine is the left atrial and ventricular wall. The wall regions of this model are defined and set to ‘wall’. At the physical viewpoint, the ‘wall’ condition was set as stationary (velocity at wall is zero), rigid with no slip condition. Figure 3 shows the faces of the 3D model that were selected as inlet, outlet, wall, fluid domain and FSI region.

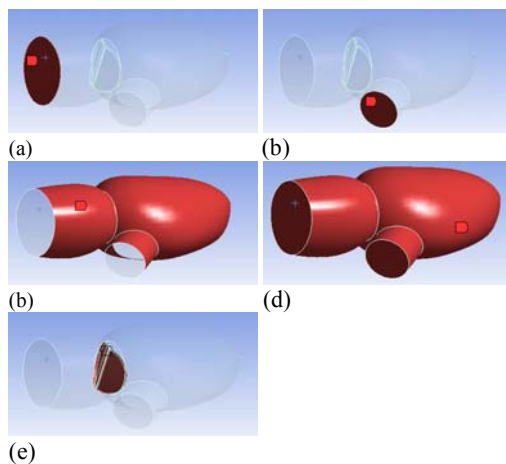


Fig. 3. Selected faces and regions for – (a) Inlet region; (b) Outlet region; (c) Wall heart region; (d) Fluid domain region; (e) FSI region

2.3 Dynamic Mesh Development

Smoothing method

Diffusion-based smoothing is integrated in the dynamic mesh. It tends to produce better quality meshes than spring-based smoothing and often allows larger boundary deformation before breaking down. For diffusion-based smoothing, the mesh motion is governed by the diffusion equation $\nabla \cdot (\gamma \nabla u) = 0$ where u is the mesh displacement velocity. The diffusion coefficient can be used to control how the boundary motion influences the interior mesh motion. In this simulation, the formulation for the diffusion coefficient, γ is a function of the boundary distance. The formula used is $\gamma = \frac{1}{v\alpha}$ where α is the diffusion parameter. In this simulation, α is set to be 1.4.

3-D MHV model

Basically, the model consists of two parts, which are the left heart and the bi-leaflet MHV. The model was constructed by using SolidWorks as an alternative from using the real left heart valve which was scanned by a 3-D scanner. The reason for this manner are the scanned models contain uneven surfaces and irregular geometry which causes difficulty for the assembly process of the heart and MHV. In addition, the irregular geometry will create complex mesh and affects the

computational time.

Loft feature in SolidWorks were used to solve the real heart irregular geometry issue. The left heart model drawn has one inlet and one outlet. The length for the left atrium and ventricle are 50 mm and 80 mm respectively, with a diameter of 31mm for the outer ring. For the leaflets model, the initial closed position is set at 60° from the horizontal axis. Figure 4 depicted the heart and leaflets model. The complex hinge geometry from the exact model is simplified with a pin joint and a weak constraint to control the designated leaflets valve position. Pyrolytic Carbon (PyC) is used as the material for the leaflets.

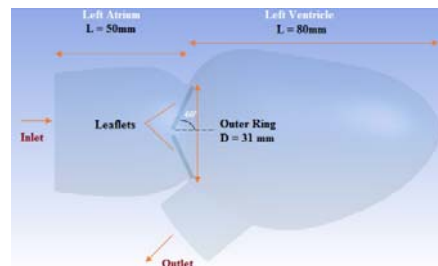


Fig. 4. Simplified CAD model for simulation with predefined dimensions

2.4 Coupling system

System coupling is a vital part in the FSI simulation as it links both the transient structural and FLUENT together to provide the final solution. Physics are coupled by passing the loads across the fluid structure interfaces where CFD transfer forces on the structure surface to the FEA. At the same time, the FEA transfer the displacements of solid structures to the CFD. Individual physics are solved separately and coupled sequentially or simultaneously until equilibrium is achieved. Figure 5 portrayed the flow of coupling system in ANSYS.

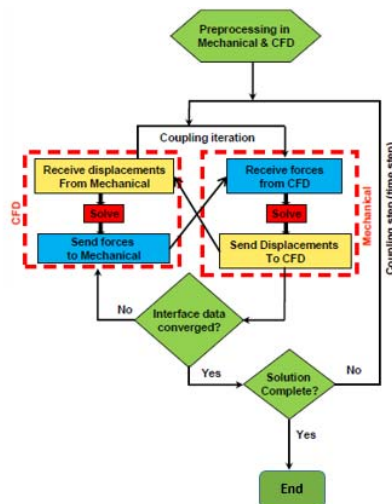


Fig. 5. Flow chart of the coupling system in ANSYS.

3. PARTICLE IMAGE VELOCIMETRY (PIV) SETUP OF BI-LEAFLET MHV

The PIV experiment comprises of the left heart

model and the bi-leaflets heart valve. Two Perspex blocks were used to create the left heart model by CNC machining while the bi-leaflets valve were fabricated using rapid prototyping machine. The assembly process of the both models was done by combining the Perspex blocks together by using bolts and nuts. Silicon sealants were applied to prevent fluid leakage. Figure 6 (a and b) showed the bi-leaflets model and Fig. 6 (c) assembled model.

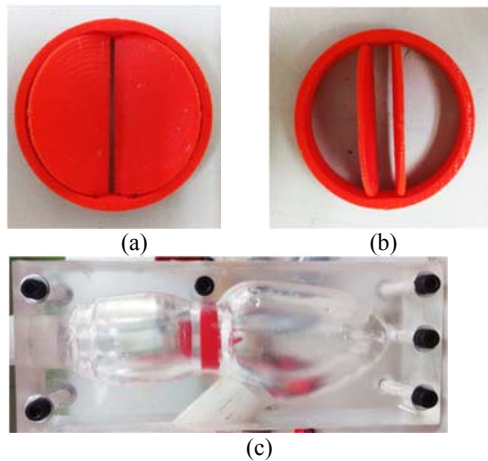


Fig. 6. Rapid prototyping bi-leaflets valve in (a) fully closed and (b) fully opened condition, and (c) the assembled model for PIV

Working Fluid

Human blood is a non-Newtonian fluid, where the viscosity of the fluid is strongly dependent on the shear rate. The dependency on the shear rate is thought to occur in a small vessel. However, in a large vessel it is acceptable to consider that blood as a Newtonian fluid. The working fluid used in the experiment to mimic human blood is an aqueous glycerol solution. The solution was prepared by mixing 22% of glycerol by mass in water. The density and kinematic viscosity of glycerol solution are 1059 kg/m^3 and $1.587 \times 10^{-6} \text{ m}^2/\text{s}$ respectively. In this experiment, 4.5 liters of glycerol was mixed with 20 liters of water. Some seeding particles (PSP-50 Polyamid from Dantec Dynamic, with diameter of $50 \mu\text{m}$ and mass of 250 g) were added in the mixture for the PIV purpose. The camera model used was Dantec HiSense MKII C8484-52-05CP Hamamatsu Digital Camera C8484-05CP with a frame rate of 12.2 fps at full resolution. Figure 7 (a) shows the schematic diagram of the PIV experiment flow system. A time interval of 1ms between pulses was used and 12 images were captured for image acquisition process.

4. RESULTS AND DISCUSSIONS

The data on the velocity contour, vector field, pressure contour, wall shear, Von Mises stress and strain are obtain through simulation process while velocity contour and vector field data are acquire from the PIV experiment. These data will be used to validate the simulation results.

4.1 Mesh Convergence Study

The mesh refinement is controlled by using relevance option. The relevance option is to enable the control of

the mesh smoothness for the entire models. In the beginning, relevance value of 0 is applied and it produces a total number of 121,903 elements in the mesh. During refine meshing, the relevance value is increase by the multiple of 10 to 60. The maximum pressure for different relevance values is tabulated in Table 1. By comparing the values in Table 1, we can see that the maximum difference between the original case and the refined cases is about 0.25%. This shows that pressure value is consistent in all cases. Similarly, in Fig. 8, mesh convergence is achieved as the pressure values do not differ much as the number of elements increased. Hence, by comparing the results, the data obtained from the original case is verified.

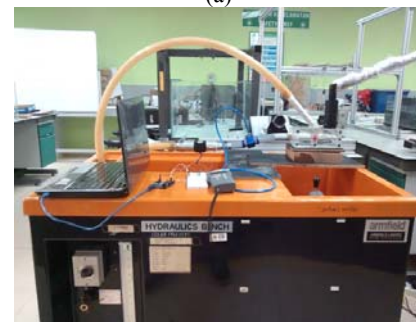
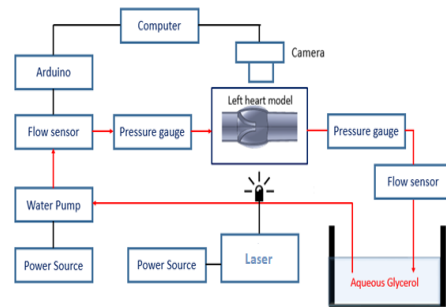


Fig. 7. (a) Schematic diagram of the flow system and (b) PIV setup in the lab

Table 1 Maximum pressure at left antrioventricular wall for different relevance

| Relevance | No of Elements | Max Pressure (Pa) | Percentage difference (%) |
|-----------|----------------|-------------------|---------------------------|
| 0 | 121903 | 16911.40 | - |
| 10 | 134503 | 16875.42 | 0.213 |
| 20 | 151123 | 16901.25 | 0.060 |
| 30 | 177750 | 16868.53 | 0.254 |
| 40 | 204135 | 16908.64 | 0.016 |
| 50 | 235993 | 16912.28 | 0.005 |
| 60 | 286375 | 16872.54 | 0.230 |

Time step

In the original calculation, the time step used is 0.01 s. For verification, a smaller time step of 0.005 s is used. The pressure at the left atrial and ventricular wall when the leaflets are fully opened is shown in Fig. 9. The maximum pressure for both cases is $1.553 \times 10^4 \text{ Pa}$ and $1.547 \times 10^4 \text{ Pa}$ respectively. The difference between the results is about 0.39%,

which implies that the pressure value is consistent and the results acquired in the original case are verified.

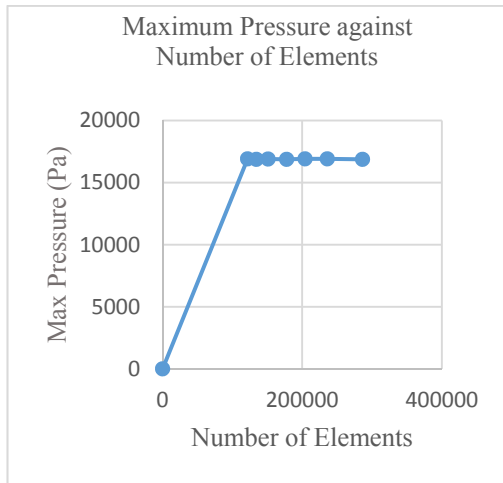


Fig. 8. Maximum pressure at left atrioventricular wall over different number of elements

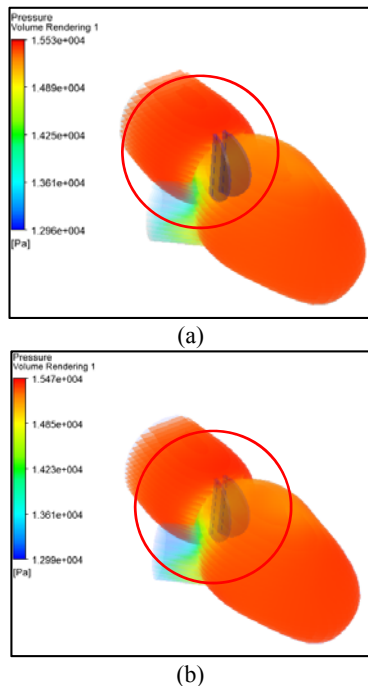


Fig. 9. Pressure at the left atrioventricular wall when the leaflets are fully opened; (a) time step = 0.01s; (b) time step = 0.005s

Experiment validation

To ensure the simulated results are reliable, comparison between simulation and experiment data are important. The velocity and vorticity are the variables that will be discussed. Figure 10 show the velocity contour and vorticity vector of both simulation and experiment respectively. The velocity contour for both simulation and experiment obtained are quite similar. In similar manner, vortex is formed at the region after the blood passes through the valves for both the simulation and experiment. Hence, it is deduced that the simulation results are accurate as it conform the experimental results.

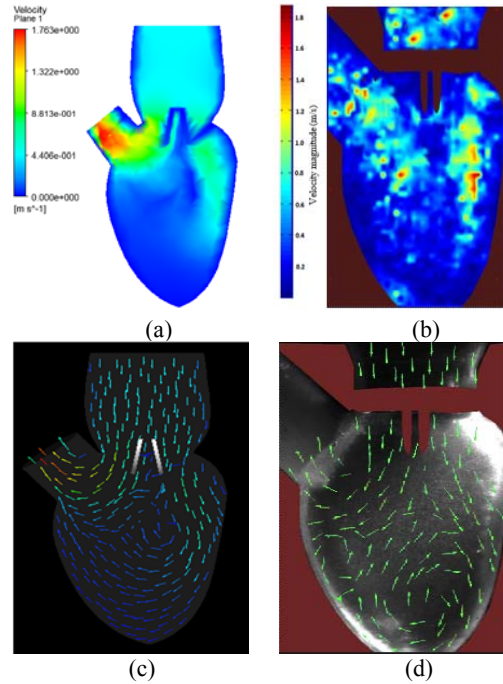


Fig. 10. Comparison between simulation and PIV experiment for velocity (a and b); and vorticity (c and d)

4.2 Velocity Contour

The velocity contour is taken at the x-y plane when the valves are fully opened. Referring to Fig. 11 (a), when the leaflets are opened, the blood flow through a central rectangular orifice and two semicircular lateral orifices. The velocity is the highest at the outlet. High velocity is observed at the region where the flow separates from the leaflet edges. The velocity at the bottom region of the heart is lower as it is further away from the outlet. Thus, the central flow is achieved and thereby improves the flow dynamic.

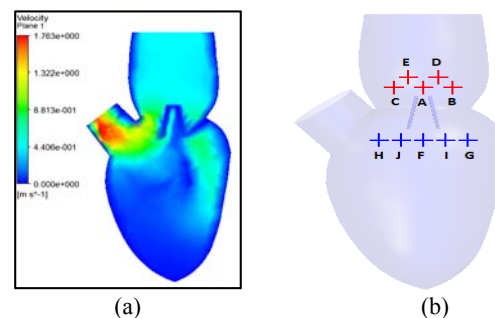


Fig. 11. (a) Velocity contour in x-y plane when the valves are fully opened; (b) selected points for velocity extraction

4.3 Doppler Velocity Index

A total of ten points are selected as shown in Fig. 11 (b), in which five points are located at the inlet region and the rest are at the outlet region. The velocities at these points will be extracted and used to calculate the Doppler velocity index. The points chosen are at critical regions which are near to the leaflets. The five points at the inlet are indicated by red cross and labeled A, B, C, D and E. The remaining points are indicated by blue cross and

labeled F, G, H, I and J. For comparison, the similar points at the same position are taken for PIV measurement. Table 2 lists the coordinates for the selected points.

Table 2 Coordinates of the selected points for data extraction

| Point | Coordinates (m) | | |
|-------|-----------------|--------|---|
| | x | y | z |
| A | 0 | 0.01 | 0 |
| B | 0.01 | 0.01 | 0 |
| C | -0.01 | 0.01 | 0 |
| D | 0.005 | 0.015 | 0 |
| E | -0.005 | 0.015 | 0 |
| F | 0 | -0.015 | 0 |
| G | 0.015 | -0.015 | 0 |
| H | -0.015 | -0.015 | 0 |
| I | 0.0075 | -0.015 | 0 |
| J | -0.0075 | -0.015 | 0 |

Doppler velocity index (DVI) is an important quantitative parameter to screen valve dysfunction. For prosthetic mitral valve, the DVI is calculated by $DVI = \frac{V_{jet}}{V_{LVO}} = \frac{V_{outlet}}{V_{inlet}}$. The DVI is calculated and tabulated in Table 3. From Fig. 12, the experimental DVI is slightly higher than the simulated DVI with the percentage difference of 14.275% (Table 3). The slight distinction is due to the constant flow rate in the experiment rather than in pulsatile condition as in the simulation. Nevertheless, the difference is not a critical issue because it is still within the allowable range for a normal prosthetic mitral valve (Table 4).

Table 3 DVI for both simulation and experiment

| Leaflets curvature | Doppler Velocity Index (DVI) | | |
|----------------------|------------------------------|------------|---------------------------|
| | Simulation | Experiment | Percentage Difference (%) |
| No curved (original) | 1.275 | 1.457 | 14.275 |

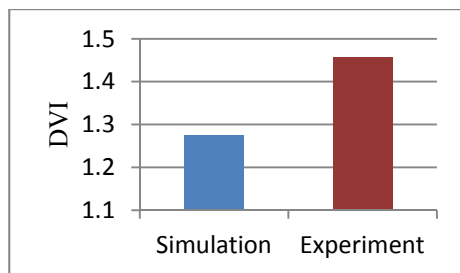


Fig. 12. Doppler velocity index for simulation and experiment

4.4 Vorticity

In fluid dynamics, a vortex is a region of a fluid where the flow rotates around an axis line. The existence of vortex increases the chance of cavitation and voids formation, thereby reducing the overall blood flow in the heart. Figure 13 presents the vorticity study at the x-y plane of the MHV using FVM and particle image velocimetry (PIV) study simulation. From Fig. 13 (a), it was shown that the computed PIV and FVM simulation results are

similar to the study by *Su et al. (2013)*. Similar vortex formation were shown when the blood flow through the fully opened valve which is expected since the vortex provides circulation of blood in a clockwise direction will redirect the inflow of blood towards the outflow tract. The location and direction of the vortex formation were also similar as observed by *Su et al. (2013)* at the vicinity of the mitral position. According to *Su et al. (2013)*, the sudden cross-sectional area expansion caused the separation of flow and formation of vortices. Additionally, the maximum velocity as recorded by *Su et al. (2013)* during the flow reaching the apex was 0.7 m/s, and is found to be in close value to the computed value of 0.61 m/s obtained in this paper. In another research, *Arefin (2017)* studied the effects of the angles between mitral and aortic orifices attained similar pattern of vortex formation, as shown in Fig. 13 (d). It can be observed that similar flow profile shown in Fig. 13 (d) as compared to our simulation and PIV data in Figs. 13 (a) and 13 (b). It is noteworthy to mention that formation of vortex is undesirable because it is capable of inducing cavitation problem which will damage the heart valve. Hence, reducing the size of the vortex will help improve the cavitation issue that MHV encounter.

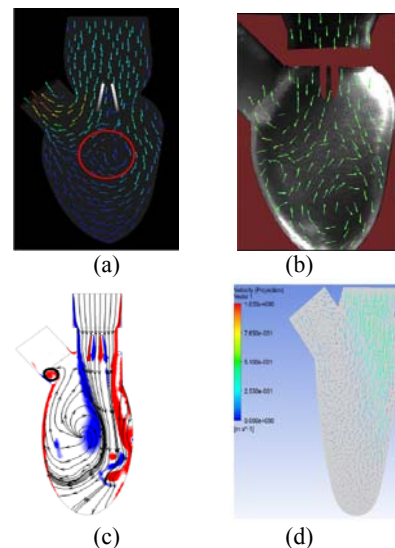


Fig. 13. Vorticity study in: (a) FVM; (b) PIV; (c) Vorticity formation obtained by *Su et al. (2013)*; (d) Vortex formation obtained from *Arefin (2017)*

4.5 Pressure Contour

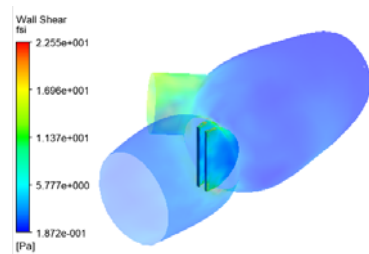
Pressure is one of the variable to capture and provide accurate estimation of blood flow in the heart. Table 5 shows the pressure contour over a cardiac cycle.

The heart valves open and close passively because of the pressure differences on either side of the valve. When the pressure is greater behind the valve, the leaflets are opened and this allow the blood to flow through it. Eventually, when the pressure is greater in front of the valve, the leaflets snap shut and the blood flow stopped. In addition, the pressure magnitudes are in the range of 120/80 mmHg (10,666 – 16,000 Pa) which is an ideal and a healthy blood pressure level for a human.

4.6 Wall Shear

Wall shear stress is the tangential drag force produced when the blood flow across the endothelial surface. The flow state was analyzed for the heart valve at the maximum opening angle. The friction between the blood and the atrial ventricular wall are highly related to the formation of blood clot. Figure 14 shows the wall shear distribution and maximum value of the wall shear.

According to Zhou *et al.* (2016), a shear stress of 100 – 500 dyne/cm² (10 – 50 Pa) greatly enhances the ability of platelets to aggregate. This will further lead to thrombosis and may endanger the patient’s life. In Fig. 14, the region near the hinge and the outer ring body are experiencing the highest wall shear stress which may trigger platelet activation. However, the damage threshold by fluid shear stress for erythrocytes (red blood cell) is 500 dyne/cm² (50 Pa) yet the maximum wall shear stress obtained is below the standard. Thus, the chance of hemolysis to occur is greatly reduced.



| Leaflets Curvature | Max wall shear stress (Pa) |
|--------------------|----------------------------|
| Original | 22.5481 |

Fig. 14. Wall shear distribution

4.7 Von Mises Stress and Strain

Von Mises stress is widely used by engineers to check their design toughness. The design will fail if the maximum value of Von Mises stress induced in the material is more than the strength of the material. Figures 15 and 16 show the Von Mises stress and strain over a cardiac cycle respectively.

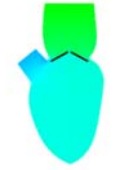
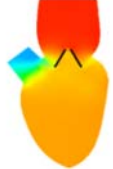
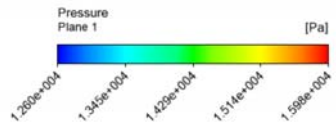
Next, the Von Mises stress and safety factor are extracted and tabulated in Table 6.

From Figs. 15 and 16, the von Mises stress and strain are the highest at time 0.02 s, which is the moment when the valve starts to open. This is because at that particular moment, the high pressure strikes large proportion of the leaflet’s surface area. The von Mises stress does not continue to increase even though the highest pressure is at time 0.1 s. The rationale behind this is that the blood flow direction is almost parallel to the surface of the leaflets, thereby giving a lower value of the von Mises stress. Afterwards, the von Mises stress undergoes a decreasing trend until time 0.4 s as the pressure starts to decrease due to better blood flow dynamic. Beyond that point, the Von Mises stress starts to hike as the pressure started to build up when the valve is fully closed. The maximum von Mises stress and strain computed using FVM simulations are found to be at the hinge area as shown in Fig. 17 (a). This is consistent with the findings from Chatpun (2013) as depicted in Fig. 17 (b) in which the maximum stress built-up was found at the hinge of the leaflets based on comparison made between bi-leaflets and tri-leaflet MHV. The results also show that the hinge experienced maximum stress during opening and closing states. In a separate study, Kadhim, Nasif, Al-Kayiem, and Al-Waked (2016) shows similar maximum von Mises stress at the hinge region during 25° and 85° opening of the bi-leaflets heart valve. They simulated those conditions with different heartbeat rate, from 80 BPM to 120 BPM. It can be concluded from Fig. 17 that the hinge joint is a critical point of concern and needs to be design properly. Even though, the design of the hinge is different, but the fact that maximum von Mises stress occurred at the high area, in this study and others (Samar Abbas, Nasif, Meor Said, Al-Waked, & Kadhim, 2017), proved that the current FVM simulation is accurate in the detection of stresses. This region should be paid more attention by MHV designers of the MHV

Table 4 Doppler velocity index for a normal prosthetic mitral valve

| | Normal | | Possible stenosis | | Significant stenosis | |
|---|---------------------------|----------------|----------------------------|------------------|----------------------|------------------|
| | Aortic | Mitral | Aortic | Mitral | Aortic | Mitral |
| Valve structure and motion | | | | | | |
| Mechanical and bio-prosthetic valve | Normal | Normal | Often abnormal | Often abnormal | Abnormal | Abnormal |
| Peak velocity (m/s) | <3 | <1.9 | 3 – 4 | 1.9 – 2.5 | >4 | >2.5 |
| Doppler velocity index | ≥0.30 | <2.2 | 0.25 – 0.29 | 2.2 – 2.5 | <0.25 | >2.5 |
| Effective orifice area (cm ²) | >1.2 | ≥2 | 0.8 – 1.2 | 1 – 2 | <0.8 | <1 |
| Effective orifice area vs. normal reference value | Reference ±1SD | Reference ±1SD | <Reference – 1SD | <Reference – 1SD | <Reference – 2SD | <Reference – 2SD |
| Contour of the transprosthetic jet | Triangular, early peaking | – | Triangular to intermediate | – | Rounded, symmetrical | – |
| Acceleration time (ms) | <80 | – | 80 – 100 | – | >100 | – |
| Pressure half time (ms) | – | <130 | – | 130 – 200 | – | >200 |

Table 5 Development of pressure contours over a cardiac cycle

| Time (s) | Pressure contour (Pa) | Time (s) | Pressure contour (Pa) |
|----------|--|--|---|
| 0 |  | 0.3 |  |
| 0.1 |  | 0.4 |  |
| 0.15 |  | 0.5 |  |
| 0.2 |  |  | |

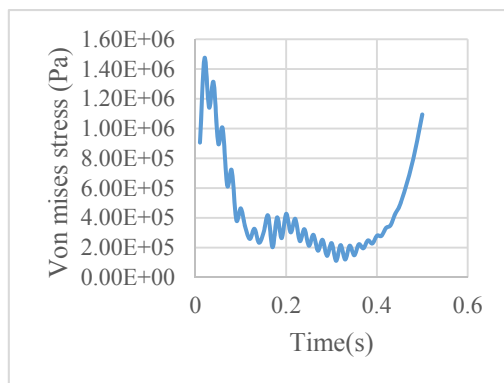


Fig. 15. Von Mises stress over a cardiac cycle

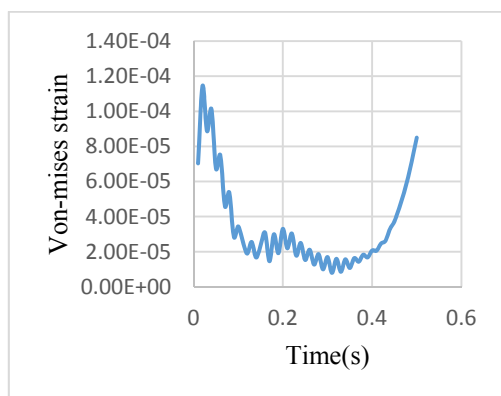


Fig. 16. Von Mises strain over a cardiac cycle

Table 6. Maximum Von Mises stress and safety factor

| Leaflets curvature | Max Von Mises Stress (MPa) | Safety factor |
|----------------------|----------------------------|---------------|
| No curved (original) | 1.47 | 15 |

5 CONCLUSION

The study investigates, using FVM and PIV approach, the blood flow through the artificial heart valve. The formation and distribution of the fluid flow, including the velocity, vorticity, pressure, and wall shear stress were analyzed in pulsating flow conditions in the numerical simulation. Not only that, the Von Mises stress, strain and safety factor of the MHV were also evaluated. The numerical results were stored and compared with the experimental data. During the experiment, the leaflets kinematics and the flow field are obtained via PIV technique. The results on velocity contour and vorticity reveal a great similarity between the numerical solution and the experimental test. The vorticity was found to be formed when the blood flow through the fully opened valve. The maximum shear stress obtained was 22.5481 Pa, near the hinge and outer ring areas. Even though the shear stress developed was below the damage threshold (50 Pa), but it is still in the range where there is high possibility of platelets aggregation. The highest Von Mises stress and strain were found in the hinge region with magnitude of 1.47 MPa and 1.19×10^{-4} respectively. Therefore, it is concluded that

the FSI algorithm is able to capture accurately all the major leaflet kinematics and dynamics, and thus can be utilized to study and optimize MHV.

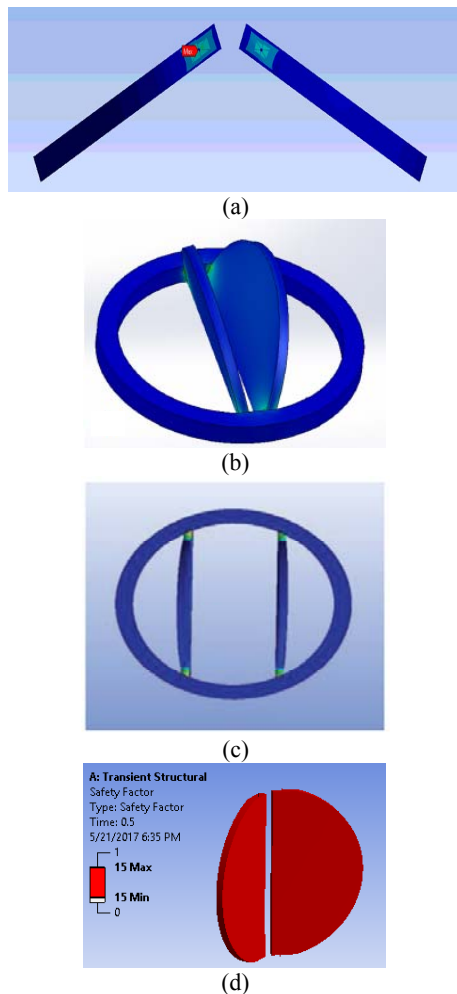


Fig. 17. (a) maximum Von Mises stress at the hinge area; (b) Chatpun (2013) finding on von Mises stress; (c) Samar Abbas *et al.* (2017) result on von Mises stress at hinge of bi-leaflet; (c) safety factor of the heart valve

Conflict of Interest

The authors declare that there is no conflict of interest regarding the publication of this paper.

Competing interests: None declared

Funding: None

Ethical approval: This research has been approved by Human Research Ethics Committee USM (HREC)

REFERENCES

Al-Atabi, M., & Lim, Y. (2013). *Investigation of Blood Flow through the Mitral Valve* (Vol. 9).
 Annerel, S., Claessens, T., Degroote, J., Segers, P., & Vierendeels, J. (2014). Validation of a numerical FSI simulation of an aortic BMHV by in vitro PIV experiments. *Medical Engineering & Physics*, 36(8), 1014-1023.

Arefin, M. S. (2017). An investigation on the effects of the angles between the mitral and aortic orifice during diastolic period using FSI. *Pathophysiology*.

Bark, D. L., Yousefi, A., Forleo, M., Vaesken, A., Heim, F., & Dasi, L. P. (2016). Reynolds shear stress for textile prosthetic heart valves in relation to fabric design. *Journal of the Mechanical Behavior of Biomedical Materials*, 60, 280-287.

Chatpun, A. K.-i. S. (2013). Mechanical analysis of mechanical aortic heart valve: Trileaflet versus bileaflet. *The 6th 2013 Biomedical Engineering International Conference*, 1-4.

Dangas, G. D., Weitz, J. I., Giustino, G., Makkar, R., & Mehran, R. (2016). Prosthetic Heart Valve Thrombosis. *Journal of the American College of Cardiology*, 68(24), 2670-2689.

Del Gaudio, C., Gasbarroni, P. L., & Romano, G. P. (2016). Experimental investigations on the fluid-mechanics of an electrospun heart valve by means of particle image velocimetry. *Journal of the Mechanical Behavior of Biomedical Materials*, 64, 229-239.

Ducci, A., Pirisi, F., Tzamtzis, S., & Burriesci, G. (2016). Transcatheter aortic valves produce unphysiological flows which may contribute to thromboembolic events: An in-vitro study. *Journal of biomechanics*, 49(16), 4080-4089.

Harris, C., Croce, B., & Cao, C. (2015). Tissue and mechanical heart valves. *Annals of Cardiothoracic Surgery*, 4(4), 399-399.

Hedayat, M., Asgharzadeh, H., & Borazjani, I. (2017). Platelet activation of mechanical versus bioprosthetic heart valves during systole. *Journal of biomechanics*, 56, 111-116.

Hong, T., & Kim, C. N. (2011). A numerical analysis of the blood flow around the Bileaflet Mechanical Heart Valves with different rotational implantation angles. *Journal of Hydrodynamics, Ser. B*, 23(5), 607-614.

Kadhim, S., Nasif, M., Al-Kayiem, H., & Al-Waked, R. (2016). *Using fluid structure interaction technique to investigate the effect of vibration on bileaflet mechanical heart valve deformation* (Vol. 11).

Kaminsky, R., Kallweit, S., Rossi, M., Morbiducci, U., Scalise, L., Verdonck, P., & Tomasini, E. P. (2008). PIV Measurements of Flows in Artificial Heart Valves *Particle Image Velocimetry: New Developments and Recent Applications* (pp. 55-72). Berlin, Heidelberg: Springer Berlin Heidelberg.

Le, T. B., & Sotiropoulos, F. (2013). Fluid-structure interaction of an aortic heart valve prosthesis driven by an animated anatomic left ventricle. *Journal of Computational Physics*, 244, 41-62.

Luraghi, G., Wu, W., De Gaetano, F., Rodriguez Matas, J. F., Moggridge, G. D., Serrani, M., . . .

- Migliavacca, F. (2017). Evaluation of an aortic valve prosthesis: Fluid-structure interaction or structural simulation? *Journal of biomechanics*, 58, 45-51.
- Misawa, Y. (2015). Valve-related complications after mechanical heart valve implantation. *Surgery Today*, 45(10), 1205-1209.
- Mokhtar, N. H., Abas, A., Teong, S. L., & Razak, N. A. (2016). Particle image velocimetry experiment of blood flow through stent in artery bifurcation aneurysm problem. *AIP Conference Proceedings*, 1775(1), 030095.
- Nguyen, V.-T., Kuan, Y. H., Chen, P.-Y., Ge, L., Sotiropoulos, F., Yoganathan, A. P., & Leo, H. L. (2012). Experimentally Validated Hemodynamics Simulations of Mechanical Heart Valves in Three Dimensions. *Cardiovascular Engineering and Technology*, 3(1), 88-100.
- Samar Abbas, S., Nasif, M., Meor Said, M. A., Al-Waked, R., & Kadhim, S. (2017). *Numerical investigation on effect of leaflet thickness on structural stresses developed in a bileaflet mechanical heart valve for its sustainable manufacturing* (Vol. 131).
- Sato, M., Harasaki, H., Wika, K. E., Soloviev, M. V., & Lee, A. S. (2003). Blood Compatibility of a Newly Developed Trileaflet Mechanical Heart Valve. *ASAIO Journal*, 49(1), 117-122.
- Sinnott, M., Cleary, P., & Prakash, M. (2006). *An investigation of pulsatile blood flow in a bifurcation artery using a grid-free method*. Paper presented at the Fifth international conference on CFD in the process industries Melbourne, Australia
- Su, B., Zhong, L., Cui, F., Gideon Praveen, K., Hui Qun, P., Kim Fatt Jimmy, H., & Leo, H. (2013). *FSI Modeling of Prosthetic Mitral Valve Dynamics and Left Ventricular Flow during Diastole*.
- Su, B., Zhong, L., Wang, X.-K., Zhang, J.-M., Tan, R. S., Allen, J. C., . . . Leo, H. L. (2014). Numerical simulation of patient-specific left ventricular model with both mitral and aortic valves by FSI approach. *Computer Methods and Programs in Biomedicine*, 113(2), 474-482.
- Zhou, F., Cui, Y. Y., Wu, L. L., Yang, J., Liu, L., Maitz, M. F., . . . Huang, N. (2016). Analysis of Flow Field in Mechanical Aortic Bileaflet Heart Valves Using Finite Volume Method. *Journal of Medical and Biological Engineering*, 36(1), 110-120.